Journal of Colloid and Interface Science **232,** 186–197 (2000)
doi:10.1006/jcis.2000.7153, available online at http://www.idealibrary.com on IDEAL®

An Improved Method of Determining the ζ-Potential and Surface Conductance

David Erickson,* Dongqing Li,*,[1] and Carsten Werner†

*Department of Mechanical & Industrial Engineering, University of Toronto, Toronto, Ontario, Canada M5S 3G8; and †Institute for Polymer Research Dresden, Dresden, Germany

Received June 20, 2000; accepted August 4, 2000

In the classical "slope–intercept" method of determining the zeta potential and the surface conductance, the relationship between ΔP and E_s is measured experimentally at a number of different channel sizes (e.g., the height of a slit channel, h). The parameter $(\varepsilon_r\varepsilon_0\Delta P/\mu E_s\lambda_b)$ is then plotted as a function of $1/h$ and linear regression is performed. The y-intercept of the regressed line is then related to the ζ-potential and its slope to the surface conductance. However, in this classical method, the electrical double layer effect or the electrokinetic effects on the liquid flow are not considered. Consequently, this technique is valid or accurate only when the following conditions are met: (1) relatively large channels are used; (2) the electrical double layer is sufficiently thin; and (3) the streaming potential is sufficiently small that the electroosmotic body force on the mobile ions in the double layer region can be ignored. In this paper a more general or improved slope–intercept method is developed to account for cases where the above three conditions are not met. Additionally a general least-squares analysis is described which accounts for uncertainty in the measured channel height as well as unequal variance in the streaming potential measurements. In this paper, both the classical and the improved slope–intercept techniques have been applied to streaming potential data measured with slit glass channels, ranging in height from 3 μm to 66 μm, for several aqueous electrolyte solutions. The comparison shows that the classical method will always overestimate both the ζ-potential and the surface conductance. Significant errors will occur when the classical method is applied to systems with small channel heights and low ionic concentrations. Furthermore, it is demonstrated that traditional regression techniques where the uncertainty is confined only to the dependent variable and each measurement is given equal weight may produce physically inconsistent results.

Key Words: **zeta potential; surface conductance; streaming potential; microchannel flow; linear regression.**

1. INTRODUCTION

Generally, most solid surfaces have electrostatic charges when in contact with a liquid medium. If the liquid contains a very small number of ions (for instance, due to impurities), the electrostatic charge on the solid surface will attract the counterions in the liquid. The rearrangement of the charges on the solid surface and the balancing charges in the liquid is called the electrical double layer, EDL (1). Because of the electrostatic interaction, the counterion concentration near the solid surface is higher than that in the bulk liquid far away from the surface. Immediately next to the surface, there is a layer of ions that are strongly attracted to the solid surface and are immobile. This layer is called the compact layer, normally less than 1 nm thick. From the compact layer to the uniform bulk liquid, the counterion concentration gradually reduces to that of bulk liquid. Ions in this region are affected less by the electrostatic interaction and are mobile. This layer is called the diffuse layer of the EDL. The thickness of the diffuse layer depends on the bulk ionic concentration and electrical properties of the liquid, ranging from a few nanometers for high ionic concentration solutions up to several micrometers for distilled water and pure organic liquids. The boundary between the compact layer and the diffuse layer is usually referred to as the shear plane. The electrical potential at the solid–liquid surface is difficult to measure directly; however, the electrical potential at the shear plane, called the zeta (ζ) potential, is a property of the solid–liquid pair, and can be measured experimentally (1).

When a liquid is forced to flow through a microchannel under an applied hydrostatic pressure, the counterions in the diffuse layer (mobile part) of the EDL are carried toward the downstream end, resulting in an electrical current in the pressure-driven flow direction, called the streaming current. Corresponding to this streaming current, there is an electrokinetic potential called the streaming potential. This flow-induced streaming potential is a potential difference that builds up along a microchannel. This streaming potential acts to force the counterions in the diffuse layer of the EDL to move in the direction opposite to the streaming current, i.e., opposite to the pressure-driven flow direction. The action of the streaming potential will generate an electrical current called the conduction current. It is obvious that when ions move in a liquid, they will pull the liquid molecules along with them. Therefore, the conduction current will produce a liquid flow in the direction opposite to the pressure-driven flow. The overall result is a reduced flow rate in the pressure drop direction. If the reduced flow rate is compared with the flow rate

[1] To whom correspondence should be addressed. E-mail: dli@mie.utoronto.ca.

0021-9797/00 $35.00

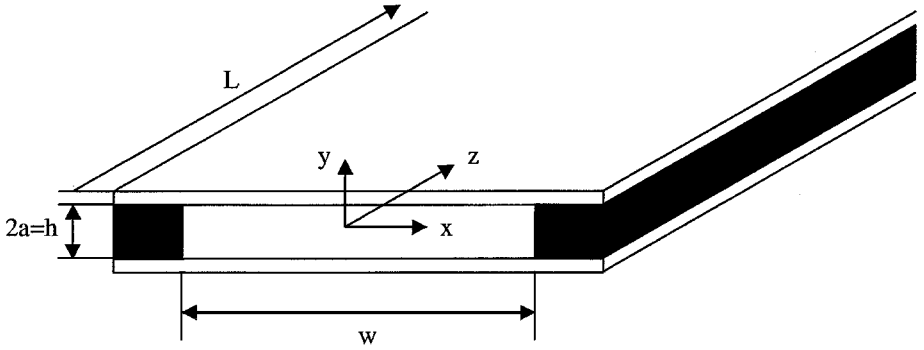

FIG. 1. Parallel plate microchannel for streaming potential measurements.

predicted by the conventional fluid mechanics theory without considering the presence of the EDL, it seems that the liquid would have a higher viscosity. This is usually referred to as the electroviscous effect (1).

In addition to the ζ-potential, another important interfacial electrokinetic parameter is the surface conductance. The surface conductance usually is referred to the electrical conductivity through a thin liquid layer near the solid–liquid interface where there is a net charge accumulation due to the charged solid–liquid interface. The ζ-potential and the surface conductance are key interfacial electrokinetic properties to a huge number of natural phenomena, such as electrode kinetics, electrocatalysis, corrosion, adsorption, crystal growth, colloid stability, and flow characteristics of colloidal suspensions and electrolyte solutions through porous media and microchannels. For example, the ζ-potential is a key parameter in determining the interaction energy between particles and hence the stability of colloid suspension systems. In electroosmotic flow or pressure-driven flow through fine capillary tubes, the ζ-potential and the surface conductance will critically influence the velocity or flow rate. In many cases, knowing the surface conductance is a must in order to evaluate the ζ-potential and other electrokinetic properties correctly.

The methods for measuring electrokinetic properties of solid–liquid interfaces generally can be classified into one of three categories: electrophoresis, electroosmosis, and streaming potential techniques (1). Electrophoresis techniques have long been popular for determining the ζ-potential of colloidal suspensions, but have also been applied to solid surfaces by crushing the surface into fine particles and then dispersing them into an aqueous solution (2). In the electroosmotic approach an electrical field is applied to the ends of a small capillary tube, resulting in a body force applied to the fluid within the double layer region near the wall. Measurements of the total volume flow rate can then be related to the ζ-potential (3). Generally very low flow rates are observed in this technique and will limit the accuracy of the measurement.

Likely the most commonly used method of measuring interfacial electrokinetic properties is the streaming potential technique. In the streaming potential technique a pressure difference, ΔP, is applied across a small channel, fine capillary, or plug depending on the application. Ions from the double layer region are transported along with the streaming solution, resulting in a streaming current, I_s, in the direction of flow. The resultant electrostatic potential or streaming potential, E_s, then induces a flow of ions in the opposite direction known as the conduction current, I_c. When the summation of the streaming and conduction current is zero the flow reaches a steady state. As will be elaborated on below, the relationship between E_s and ΔP is then used to determine the electrokinetic properties of the surface.

Figure 1 shows a flat plate or slit microchannel composed of two flat, parallel, solid surfaces between which a liquid flows. In general the height of these channels is much less than their width so that side effects can be ignored and it is customary to assume the flow as one-dimensional. Such devices are preferred for making streaming potential measurements over cylindrical capillaries since both surface treatment and quantitative analysis are greatly facilitated (4–7). Recently Werner *et al.* (8) have developed an advanced flat plate streaming device which allows adjustment of the channel height via a micrometer screw.

As mentioned earlier the streaming current is the flow of the unbalanced ions in the mobile double layer region caused by the pressure-driven liquid flow through a channel. The streaming current for a slit microchannel is defined by (referring to Fig. 1)

$$I_s = 2\int_0^a v_z(y)\rho(y)w\,dy, \qquad [1]$$

where a is the half-height of the channel, equivalent to $h/2$, w is the width, $v_z(y)$ is the velocity profile of the liquid, which varies only in the y direction for 1-D flow, and $\rho(y)$ is the volume density of the net charge across the parallel plate channel. Thus, with a knowledge of the net charge distribution and the velocity profile the streaming current can be evaluated.

For a solid surface in an infinite liquid medium, the distribution of volume density of the net charge in the EDL is described by the Poisson–Boltzmann equation, which for the case being considered here takes the form

$$\frac{d^2\psi}{dy^2} = -\frac{\rho(y)}{\varepsilon_r\varepsilon_o}, \qquad [2]$$

where ε_o is the electrical permittivity of a vacuum, ε_r is the relative dielectric constant of the liquid, and ψ is the electrical potential at a distance y from the shear layer. Substituting the above into Eq. [1] yields

$$I_s = -2w\varepsilon_r\varepsilon_o \int_0^a v_z \frac{d^2\psi}{dy^2}\, dy. \quad [3]$$

To evaluate Eq. [3] the integration by parts method is used as below,

$$I_s = -2w\varepsilon_r\varepsilon_o \left(v_z \frac{d\psi}{dy}\bigg|_{y=0.}^{y=a} - \int_{y=0}^{y=a} \frac{d\psi}{dy}\, dv_z \right). \quad [4]$$

The first term in brackets in Eq. [4] is equal to zero since $d\psi/dy = 0$ when $y = 0$ and $v_z = 0$ when $y = a$. Thus Eq. [4] reduces to

$$I_s = 2w\varepsilon_r\varepsilon_o \int_{y=0}^{y=a} \frac{d\psi}{dy}\, dv_z. \quad [5]$$

The second piece of information required to evaluate the streaming current is a description of the velocity profile. Although Eq. [5] is evaluated over the entire half-height of the channel it is important to note that $d\psi/dy$ is negligible everywhere except in the double layer region near the solid surface. As such this is the critical region where the velocity profile must be accurately known.

In the classical approach to this problem it is customary to determine the velocity profile from the Navier–Stokes equation for momentum by considering the pressure drop as the only motive force (i.e., ignoring any body forces which may be caused by electrokinetic effects). Using this approach for the parallel plate geometry, Eq. [6] is obtained,

$$\mu \frac{d^2 v_z}{dy^2} - \frac{dP}{dz} = 0, \quad [6]$$

where μ is the viscosity and dP/dz describes the change in pressure along the z-axis and is usually approximated as $-\Delta P/L$, where ΔP is the total pressure drop and L is the length of the channel. The solution to Eq. [6] can be found quite easily by applying the no-slip boundary condition at the shear plane, i.e., $v_z = 0$ at $y = \pm a$, and is well known as the Hagen–Poiseuille or parabolic flow profile given by Eq. [7],

$$v_z = \frac{\Delta P}{L}\frac{a^2}{2\mu}\left(1 - \frac{y^2}{a^2}\right). \quad [7]$$

Since the velocity profile is required only in the thin region near the surface it is customary to further simplify Eq. [7], allowing for easier integration of Eq. [5],

$$v_z = \frac{\Delta P}{L}\frac{a^2}{2\mu}\left(1 - \frac{y}{a}\right)\left(1 + \frac{y}{a}\right) \approx \frac{\Delta P}{L}\frac{a^2}{\mu}\left|1 - \frac{y}{a}\right|, \quad [8]$$

thus leaving a simple linear approximation to the velocity profile in the EDL. It should be realized that the above velocity profile is obtained without considering the EDL or electrokinetic effect on the liquid flow in the fine capillary. Therefore, it is not difficult to understand that for smaller channels and thicker electrical double layers the error in Eq. [8] becomes severe.

Taking the derivative of Eq. [8], substituting it into Eq. [5], and applying the boundary conditions $\psi(y = 0) = \zeta$ and $\psi(y = a) = 0$ yields

$$I_s = -\frac{2wa\varepsilon_r\varepsilon_o\Delta P}{\mu L}\int_{y=0}^{y=a} d\psi = -\frac{2wa\varepsilon_r\varepsilon_o\Delta P}{\mu L}(\psi|_{y=a} - \psi|_{y=0})$$
$$= -\frac{2wa\varepsilon_r\varepsilon_o\Delta P\zeta}{\mu L}. \quad [9]$$

As mentioned earlier the flow-induced streaming potential produces a conduction current in the direction opposite to the flow, given by

$$I_c = A_c\lambda_b\frac{E_s}{L} + P_w\lambda_s\frac{E_s}{L} = \left(\lambda_b + \lambda_s\frac{P_w}{A_c}\right)A_c\frac{E_s}{L}, \quad [10]$$

where A_c and P_w are the cross-sectional area and wetted perimeter of the channel, λ_b is the bulk conductivity, and λ_s is the surface conductivity.

In the 1930s and even earlier, authors such as Briggs (9) recognized that the dependence of ζ-potential on the radius of the capillary tube was likely the result of a surface conductance effect. At the time this result and interpretation were not universally accepted and there was some debate as to whether the ζ-potential was truly a material- and condition-specific characteristic. In his pioneering work, Rutgers (10) developed a relationship between the surface, bulk, and total conductivity of a solid–liquid flow system which led to the above form of Eq. [10]. For a parallel plate channel with $w \gg a$, such as that shown in Fig. 1, $P_w/A_c \approx 2/h$, so Eq. [10] reduces to the slightly simpler form shown below,

$$I_c = 2aw\left(\lambda_b + \frac{2\lambda_s}{h}\right)\frac{E_s}{L}. \quad [11]$$

An important consequence of Eq. [11] is that for large channels, such as when $h > 200\ \mu$m, surface conductance effects can be ignored.

For steady-state flow, $I_c + I_s = 0$. Inserting Eq. [9] and Eq. [11] into this condition yields the following expression,

$$\frac{E_s}{\Delta P} = \frac{\varepsilon_r\varepsilon_o\zeta}{\mu}\frac{1}{(\lambda_b + 2\lambda_s/h)}. \quad [12]$$

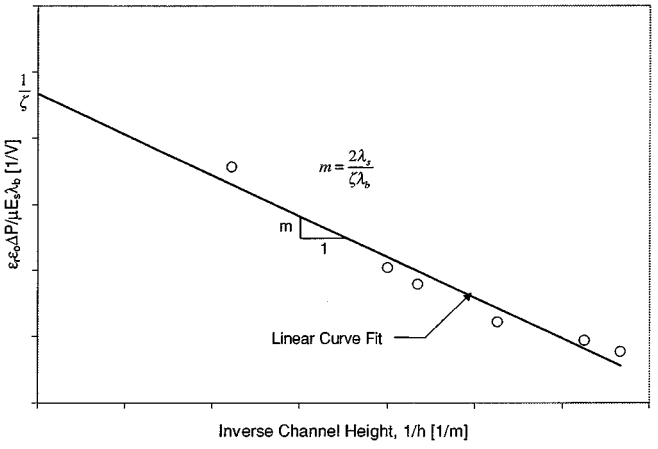

FIG. 2. Determination of the ζ-potential and λ_s by using the streaming potential data and the slope–intercept method.

It is this form of the equation, or some variation thereof, that is the basis for the evaluation of the electrokinetic properties of a solid surface from streaming potential measurements.

Eq. [12] can be expanded and rearranged into the form shown below,

$$\frac{\varepsilon_r\varepsilon_o\Delta P}{\mu E_s\lambda_b} = \frac{1}{\zeta} + \left(\frac{2\lambda_s}{\zeta\lambda_b}\right)\frac{1}{h}. \qquad [13]$$

Using Eq. [13] a "slope–intercept" method was developed to determine both the ζ-potential and λ_s by measuring ΔP and E_s at different channel heights. In the classical form of this technique the relationship between ΔP and E_s is measured experimentally at a number of different channel sizes. The parameter $\varepsilon_r\varepsilon_o\Delta P/\mu E_s\lambda_b$ is then plotted as a function of $1/h$ and linear regression is performed as shown in Fig. 2. According to Eq. [13], the y-intercept of the regressed line is then related to the ζ-potential and its slope to the surface conductance.

As pointed out earlier, the derivation of Eq. [12] and Eq. [13] did not consider the electrokinetic or EDL effects on the flow. The applicability of these equations therefore is limited to large channel systems. In other words the accuracy of Eq. [12] and thus Eq. [13] is dependent on the following three conditions:

(1) The channel size must be relatively large.

(2) In comparison with the channel size, the double layer must be sufficiently thin that the velocity profile remains essentially linear for the entire channel cross section.

(3) The streaming potential is sufficiently small that the electroosmotic body force on the mobile ions in the double layer region can be ignored.

It should be noted that these three conditions are often related. For example, in a high ionic concentration solution flowing through a microchannel, both EDL thickness and streaming potential are small. In the case of low concentration solutions and small channels, the double layer is relatively thick and the streaming potential is relatively large. In the latter of these situations Eq. [12] and Eq. [13] are likely to be at best in error and at worst invalid.

In this paper the classical slope–intercept method for determining the ζ-potential and surface conductance of a solid surface will be extended to account for cases where the above conditions are not met. As will be shown below, this was done by the addition of a correction factor applied to the left-hand side of Eq. [13] to account for deviations from conditions 1 and 2 and a slope correction which accounts for cases where condition 3 is not met. Additionally a general least-squares analysis is described which accounts for uncertainty in the measured channel height as well as unequal variance in the streaming potential measurements. The improved slope–intercept technique will be compared with the classical method and shown to have dramatic effects when the channel height is small and/or the solution's ionic concentration is low.

In this paper, both the classical and modified slope–intercept techniques have been applied to streaming potential data measured for glass surfaces at channel heights ranging from 3 μm to 66 μm, for three streaming solutions of differing ionic concentrations. As will be shown the classical method will always overestimate both the ζ-potential and surface conductance. Additionally it is demonstrated that traditional regression techniques where the uncertainty is confined to the dependent variable and each measurement is given equal weight may well produce physically inconsistent results.

2. IMPROVED SLOPE–INTERCEPT TECHNIQUE

As discussed above, the premise on which the classical method is built is largely dependent on the assumption of negligible EDL effect on the flow. It has long been known that this is generally not the case for small channels with aqueous solutions of a low ionic concentration. Since the key reason for ignoring corrections to the classical equations is the increased complexity of the mathematical analysis, the major purpose of this paper is to propose a simple method by which the slope–intercept method can be extended to account for the more general cases.

To begin, the Navier–Stokes equation [7] is modified to account for the additional body force caused by the streaming potential acting on the ions in the mobile or diffuse part of the double layer region,

$$\mu\frac{d^2v_z}{dy^2} - \frac{dP}{dz} + \frac{E_s}{L}\rho(y) = 0. \qquad [14]$$

Substituting Eq. [2] for $\rho(y)$ as before and again assuming a linear pressure drop across the channel, Eq. [15] is obtained,

$$\frac{d^2v_z}{dy^2} = \frac{\varepsilon_r\varepsilon_o E_s}{\mu L}\frac{d^2\psi}{dy^2} - \frac{\Delta P}{\mu L}. \qquad [15]$$

Integrating Eq. [15] twice yields

$$v_z(y) = \frac{\varepsilon_r\varepsilon_o E_s}{\mu L}\psi(y) - \frac{\Delta P}{\mu L}\frac{y^2}{2} + c_1y + c_2. \qquad [16]$$

The constants of integration in Eq. [16] can be determined by applying the no-slip boundary conditions at the beginning of the shear plane, $y = \pm a$, $\psi(0) = \zeta$, $v_z(0) = 0$, yielding Eq. [17],

$$v_z(y) = \frac{\Delta P a^2}{2\mu L}\left(1 - \frac{y^2}{a^2}\right) - \frac{\varepsilon_r \varepsilon_o E_s \zeta}{\mu L}\left(1 - \frac{\psi(y)}{\zeta}\right). \quad [17]$$

It is important to note that up to this point no simplifying assumptions have been made. However, unlike in Section 1, to completely define the velocity profile an expression for $\psi(y)$ is required. To obtain such an expression, an analytical solution to Eq. [2] is necessary.

For symmetric valent ions, the net charge density in Eq. [2] is given by the Boltzmann equation as

$$\rho = (n^+ - n^-)ze = -2n_o ze \sinh\left(\frac{ze\psi}{k_b T}\right), \quad [18]$$

where n_o is the bulk ionic concentration, z is the valence of the ion, e is the charge of an electron, k_b is the Blotzmann constant, and T is the absolute temperature. Substituting Eq. [18] into Eq. [2] yields

$$\frac{d^2\psi}{dy^2} = \frac{2}{\varepsilon_r \varepsilon_o} n_o ze \sinh\left(\frac{ze\psi}{k_b T}\right). \quad [19]$$

Unfortuately, even for a flat surface, the general analytical solution of Eq. [20] does not present $\psi(y)$ in the explicit form needed to obtain an analytical solution of Eq. [17]. Therefore, a linear assumption referred to as the Debye–Huckel approximation was used here to simplify Eq. [19]. Assuming $|ze\psi/k_b T| < 1$, Eq. [19] reduces to

$$\frac{d^2\psi}{dy^2} = \kappa^2 \psi \quad [20a]$$

$$\kappa = \left(\frac{2n_o z^2 e^2}{\varepsilon_r \varepsilon_o k_b T}\right)^{1/2}, \quad [20b]$$

where κ is the Debye–Huckel parameter; $1/\kappa$ is often referred to as the characteristic thickness of the double layer. The applicability of the Debye–Huckel approximation has been discussed by a number of authors. Hunter (1) states that in general the approximation is valid when ζ is less than about 25 mV at room temperature; however, for situations like the flow-through capillaries this approximation may be valid for ζ as high as 100 mV.

Equation [20] can be solved by applying the boundary conditions $y = \pm a$, $\psi = \zeta$ and $y = 0$, $\psi = 0$, yielding

$$\psi(y) = \frac{\zeta}{\sinh(\kappa a)} |\sinh(\kappa y)|. \quad [21]$$

Substituting Eq. [21] into Eq. [17] yields the final equation describing the 1-D velocity profile of a solution through a parallel plate microchannel with the electrokinetic or electroviscous effect on the flow,

$$v_z(y) = \frac{\Delta P a^2}{2\mu L}\left(1 - \frac{y^2}{a^2}\right) - \frac{\varepsilon_r \varepsilon_o E_s \zeta}{\mu L}\left(1 - \frac{|\sinh(\kappa y)|}{\sinh(\kappa a)}\right). \quad [22]$$

From Eq. [22] it is apparent that the second term accounts for the electrokinetic or the electroviscous effect on the flow, and when $\zeta = 0$ or $E_s = 0$, the velocity profile reduces to the Hagen–Poiseuille solution described in Section 1, Eq. [7].

Using the form of the velocity profile given in Eq. [17], the streaming current can be evaluated from Eq. [5] as

$$I_s = 2w\varepsilon_o \varepsilon_r \left(-\frac{\Delta P}{\mu L}\int_{y=0}^{y=a} y\frac{d\psi}{dy}\,dy + \frac{\varepsilon_o \varepsilon_r E_s}{\mu L}\int_{y=0}^{y=a}\left(\frac{d\psi}{dy}\right)^2 dy\right). \quad [23]$$

The two integrals in the above equation can then be evaluated by making use of Eq. [21],

$$\int_{y=0}^{y=a} y\left(\frac{d\psi}{dy}\right) dy = \zeta a\left(1 - \frac{\cosh(\kappa a) - 1}{\kappa a \sinh(\kappa a)}\right) \quad [24a]$$

$$\int_{y=0}^{y=a}\left(\frac{d\psi}{dy}\right)^2 dy = \left(\frac{\zeta\kappa}{\sinh(\kappa a)}\right)^2\left(\frac{\sinh(\kappa a)\cosh(\kappa a)}{2\kappa} + \frac{a}{2}\right). \quad [24b]$$

Thus, the final solution for the streaming current is given by

$$I_s = -\frac{2w\varepsilon_r \varepsilon_o}{\mu L}\left(\Delta P \zeta a \beta_1 - \frac{E_s \varepsilon_r \varepsilon_o \zeta^2}{a}\beta_2\right) \quad [25a]$$

$$\beta_1 = 1 - \frac{\cosh(\kappa a) - 1}{\kappa a \sinh(\kappa a)} \quad [25b]$$

$$\beta_2 = \left(\frac{\kappa a}{\sinh(\kappa a)}\right)^2\left(\frac{\sinh(\kappa a)\cosh(\kappa a)}{2\kappa a} + \frac{1}{2}\right). \quad [25c]$$

Using Eq. [25a], Eq. [11], and the steady-state condition $I_s + I_c = 0$, a more general form of the Smoluchowski equation is obtained,

$$\frac{E_s}{\Delta P} = \frac{\varepsilon_r \varepsilon_o \zeta}{\mu(\lambda_b + 2\lambda_s/h)}\Phi_P \quad [26a]$$

$$\Phi_p = \frac{\beta_1}{1 + \frac{\beta_2(\varepsilon_r \varepsilon_o)^2 \zeta^2}{a^2 \mu(\lambda_b + 2\lambda_s/h)}}. \quad [26b]$$

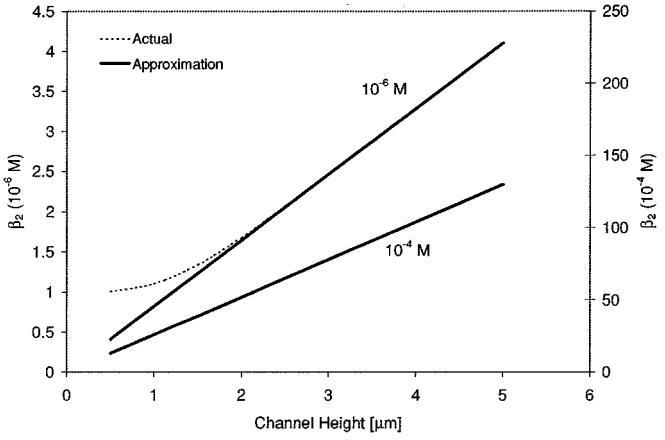

FIG. 3. Relationship between approximated and actual values of β_2 for parallel plate channels.

2.1. Improved Slope–Intercept Method

The simplification of Eq. [26] begins by recognizing the following identity,

$$\lim_{x\to\infty} \frac{\cosh(x)}{\sinh(x)} = 1. \qquad [27]$$

By applying Eq. [27] to Eq. [25c], β_2 can be simplified to yield

$$\beta_2 = \left(\frac{\kappa a}{\sinh(\kappa a)}\right)^2 \left(\frac{\sinh(\kappa a)\cosh(\kappa a)}{2\kappa a} + \frac{1}{2}\right) \approx \frac{\kappa a}{2}. \qquad [28]$$

The range where such an approximation is valid is actually quite large as seen in Fig. 3. For the extreme case of pure water (10^{-6} M) the approximation converges to within 99% of the actual value at all channel heights greater than 2.3 μm. At smaller channel heights the divergence is quite rapid, and users of this technique should be aware of this limitation when κa is very small.

With the above approximation, Eq. [26] reduces to

$$\frac{E_s}{\Delta P} = \frac{\varepsilon_o \varepsilon_r \zeta}{\mu(\lambda_b + 2\lambda_s/h)} \frac{\beta_1}{1 + \frac{\kappa(\varepsilon_r\varepsilon_o)^2\zeta^2}{2a\mu(\lambda_b + 2\lambda_s/h)}}, \qquad [29]$$

which can be rearranged into a form similar to that of Eq. [13] as shown below,

$$\beta_1 \frac{\varepsilon_r \varepsilon_o \Delta P}{\mu \lambda_b E_s} = \frac{1}{\zeta} + \left(\frac{2\lambda_s}{\zeta\lambda_b} + \frac{\kappa(\varepsilon_r\varepsilon_o)^2\zeta}{\mu\lambda_b}\right)\frac{1}{h}. \qquad [30]$$

Equation [30] is the final form of the equation for the improved slope–intercept method.

By comparing Eq. [30] with Eq. [13] (the equation for the classical method), the differences and similarities are apparent. The above form of the equation still allows for the same graphical technique to be used as before to determine ζ and λ_s; however, the β_1 correction factor must be applied to the left-hand side. The value of the slope correction, $\kappa(\varepsilon_r\varepsilon_o)^2\zeta/\mu\lambda_b$, must be subtracted from the slope of the best-fit line before it is used to determine the surface conductance.

2.2. Physical Significance of the Modifying Factors

The β_1 modifying factor is a function of only the Debye–Huckel parameter and the channel height. The value of this parameter characterizes the effects of channel height relative to the EDL thickness. Physically it would be expected that as the channel height decreases or the double layer thickness increases, which is equivalent to κa decreasing, this effect should become more pronounced. This is confirmed in Fig. 4 where it is apparent that as channel height and ionic concentration increase, β_1 approaches unity and thus Eq. [30] reverts to Eq. [13]. From Fig. 4 it is apparent that at small channels in pure water the magnitude of β_1 can be very significant, reaching as low as 0.8 when $h = 3$ μm and not reaching 99% of its final value until h is greater than 60 μm.

As a result of β_1 always being less than unity, the left-hand side of Eq. [30] will always be less than that of the classical Eq. [13]. Returning then to Fig. 2 and comparing the two methods, it is apparent that for measurements made at any real channel height the improved method will always yield a slope of lower magnitude and a y-intercept of higher magnitude (i.e., more negative). Consequently, the previous analysis done with the classical technique is likely to have predicted values of ζ and λ_s that are higher than the true values.

The slope correction factor, $\kappa(\varepsilon_r\varepsilon_o)^2\zeta/\mu\lambda_b$, is required to account for the additional body force on the ions in the double layer region, caused by the induced electrical field (i.e., streaming potential). This counter pressure, known as the electroosmotic back pressure, will result in a reduction in the flow velocity. Since the flow velocity, v_z, is reduced it is apparent from Eq. [1] that the magnitude of the streaming current will be lower, which then induces a lower streaming potential, thus increasing the ratio of $\Delta P/E_s$. The magnitude of this effect is approximately proportional to $1/h$ and as a result will lead to an increase in the

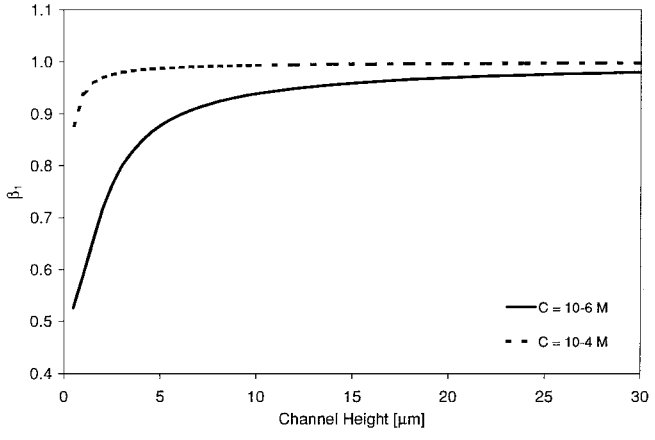

FIG. 4. β_1 correction factor as a function of channel height for different solution concentrations.

magnitude of the slope of a best-fit line, which must be accounted for before the surface conductance is calculated. An important consequence of Eq. [30] and this correction is that it suggests that even if $\lambda_s = 0$, the $\Delta P/E_s$ relationship still depends on the channel height, unlike the classical method which predicts that no such relationship should exist.

3. LEAST-SQUARES ANALYSIS

As discussed previously once the experimental data are plotted, the ζ-potential and surface conductance are determined from a best-fit line through the data points. To do so, generally a least-squares analysis is performed. It should be pointed out that how such a least-squares analysis is conducted will directly affect the accuracy of ζ and λ_s. A general technique for performing this regression will be discussed in this section.

As mentioned earlier the values of ζ and λ_s are determined from the slope and the y-intercept of a line of best fit, as shown in Fig. 2. The most common method of determining this best-fit line is through least-squares analysis, which minimizes the sum of squares of the error between the experimentally observed value and that predicted from the curve fit. Since Eq. [13] and Eq. [30] are linear equations with one independent variable, the general form of the best-fit line is given by Eq. [31],

$$y_i = \alpha_1 x_i + \alpha_2, \qquad [31]$$

where y_i and x_i are the calculated (or adjusted) values of the dependent and independent variables respectively, and α_1 and α_2 are the best-fit parameters for the slope and intercept. Since the data are likely to be at least somewhat scattered about the best-fit line, residuals are defined as below, which describe the difference between the calculated value and the measured (observed) value,

$$R_{x_i} = X_i - x_i \qquad [32a]$$

$$R_{y_i} = Y_i - y_i, \qquad [32b]$$

where R_{x_i} and R_{y_i} are the residuals and X_i and Y_i are the measured values.

To determine α_1 and α_2 the following general least-squares risk function is defined whose value is minimized when α_1 and α_2 assume their best-fit values,

$$S = \sum_{i=1}^{n} \left(w_{y_i} R_{y_i}^2 + w_{x_i} R_{x_i}^2 \right), \qquad [33]$$

where n is the number of data points. The weight functions, w_{x_i} and w_{y_i}, are given by Eq. [34a] and Eq. [34b],

$$w_{x_i} = \frac{1}{\sigma_{x_i}^2} \qquad [34a]$$

$$w_{y_i} = \frac{1}{\sigma_{y_i}^2}, \qquad [34b]$$

where σ_{x_i} and σ_{y_i} are the standard deviations of the ith measurement in the x and y directions. In general, statistical weighting is required to account for the possibility that the uncertainty in each measured value may not be constant. Wolberg (11) gives a detailed explanation of statistical weighting as well as justifications for Eq. [34a] and Eq. [34b].

It is common practice when a linear least-squares analysis is performed to make two assumptions: that the variance of all measured or dependent values is equivalent and that the error in the x or independent measurement is negligible. As a result Eq. [33] reduces to the special case and more familiar form,

$$S = \sum_{i=1}^{n} R_{y_i}^2. \qquad [35]$$

In the case considered here, the above assumptions are not necessarily justified. First there is no reason to make an *a priori* assumption that all the dependent variables will be of equal variance. Uncertainties in the $\Delta P/E_s$ relationship, for example due to electrode imbalance and changes in the bulk conductivity and viscosity due to slight temperature changes, can all contribute to the overall uncertainty to varying degrees. Statistically those data points that are known to be of a lower accuracy must be given less weight than those that are known more precisely. Additionally the effective height of the channel is never known exactly but is known to within some precision. Effects such as surface roughness, unparallelism of the plates, and uncertainty in the actual channel measurement itself can all contribute to the total uncertainty. As will be demonstrated later failure to account for these additional uncertainties can result in large errors.

3.1. Minimization of the Least-Squares Function

The method of minimizing Eq. [33] is more complicated than that for Eq. [35], but the basic algorithm is primarily the same. In both cases the approach is to find the values of the fitted parameters which make Eq. [36] equal to zero,

$$\frac{1}{2}\delta S = \sum_{i=1}^{a} \left(w_{y_i} R_{y_i} \delta R_{y_i} + w_{x_i} R_{x_i} \delta R_{x_i} \right) = 0. \qquad [36]$$

If the traditional regression approach is taken Eq. [36] is greatly simplified since $w_{y_i} = 1$ and $R_{x_i} = 0$. The main difference between the two minimization procedures is that while the traditional least-squares problem can be solved directly, the general case requires an iterative solution. The following procedure for minimization of Eq. [36] was used in this study and is suggested for use with the slope–intercept method; the mathematics of the solution are detailed in the Appendix.

(1) Initial guesses for α_1 and α_2 are made. The actual value of these guesses is not critical in the traditional method where a direct solution can be obtained; however, for the more general procedure the accuracy of the guesses can lead to convergence or divergence of the algorithm. The reader is referred to Wolberg (11) for more details.

(2) With the measured values of X_i and Y_i, the values of two functions F_i, Eq. [37a], and L_i, Eq. [37b], are computed for each data point:

$$F_i = Y_i - \alpha_1 X_i - \alpha_2 \qquad i = 1, 2, \ldots n \qquad [37a]$$

$$L_i = \sigma_{y_i}^2 + (\alpha_1 \sigma_{x_i})^2 \qquad i = 1, 2, \ldots n. \qquad [37b]$$

(3) Using F_i and L_i, the values of A_1 and A_2 are computed directly from the linear system shown below,

$$C \begin{bmatrix} A_1 \\ A_2 \end{bmatrix} = V \qquad [38a]$$

$$C = \begin{bmatrix} \sum_{i=1}^{n} \frac{X_i^2}{L_i} & \sum_{i=1}^{n} \frac{X_i}{L_i} \\ \sum_{i=1}^{n} \frac{X_i}{L_i} & \sum_{i=1}^{n} \frac{1}{L_i} \end{bmatrix} \qquad [38b]$$

$$V = -\begin{bmatrix} \sum_{i=1}^{n} \frac{X_i F_i}{L_i} \\ \sum_{i=1}^{n} \frac{F_i}{L_i} \end{bmatrix}. \qquad [38c]$$

(4) A_1 and A_2 are then used to compute the updated values of α_1 and α_2 using Eq. [39]:

$$\alpha_k|_{\text{new}} = \alpha_k|_{\text{old}} - A_k \qquad k = 1, 2. \qquad [39]$$

(5) The procedure, starting with step 2, is then repeated with the updated values of α_1 and α_2 until a convergence criterion is met. Wolberg (11) suggests the following criteria,

$$\left| \frac{\Delta \alpha_k}{\alpha_k} \right| < \epsilon \qquad k = 1, 2, \qquad [40]$$

where ϵ is a predetermined error tolerance.

3.2. Uncertainty in the Least-Squares Parameters

As with any statistical treatment of data, of utmost importance in a least-squares analysis is the uncertainty in the best-fit parameters. For the general least-squares analysis presented above the standard deviation of the best-fit parameters can be estimated from Eq. [41] (11),

$$\sigma_k \approx \left(\frac{\sum_{i=1}^{n} F_i^2 / L_i}{n-2} \right)^{1/2} \left(C_{kk}^{-1} \right)^{1/2} \qquad k = 1, 2, \quad [41]$$

where F_i and L_i are given by Eq. [37a] and Eq. [37b] evaluated at the best-fit parameters and C_{kk} is the diagonal element of the coefficient matrix Eq. [38b].

Using Eq. [41] the confidence interval on the best-fit parameters can be determined by Eq. [42],

$$a_k - \sigma_k t_{(\beta/2, n-2)} < a_k < a_k + \sigma_k t_{(\beta/2, n-2)}, \qquad [42]$$

where $t_{(\beta/2, n-2)}$ is the value of the t-statistic at a confidence level of $1 - \beta$ with $n - 2$ degrees of freedom. Equation [42] describes the range in which the actual or true values of the best-fit parameters are known to be within a confidence of $1 - \beta$.

In the following section the above regression technique and uncertainty analysis will be applied to both the classical and improved forms of the slope–intercept method for streaming potential measurements made in slit glass channels. As will be shown failure to account for the uncertainty in both the channel height and streaming potential measurements in the regression algorithm can produce inadequate results.

4. ELECTROKINETIC CHARACTERIZATION OF GLASS SURFACES

In this section the slope–intercept technique will be applied to streaming potential measurements made on glass surfaces for three different streaming solutions: pure water, 10^{-4} M KCl, and 10^{-3} M KCl aqueous solutions. A comparison will be made between the improved method and classical techniques. Additionally the results obtained using the general least-squares regression algorithm outlined in Section 3 will be compared with those obtained using the traditional least-squares regression method.

4.1. Experimental Procedure

Streaming potential measurements were carried out in the variable height parallel plate channel device described in detail by Werner *et al.* (8). This device allows adjustment of the distance between two 10 mm $\times$ 20 mm flat surfaces from over 50 μm down to 1 μm in perfect parallel position without having to remove the sample surfaces. Plate parallelism along the x and z axes, see Fig. 1, was controlled via an optical microscope. A high-pressure N_2 gas reservoir is used to produce the pressure drop across the channel which is controlled electronically by a pressure transducer and electromagnetic valve. For further details on the apparatus the reader is referred to the above reference and more information on the details of streaming potential measurements is given in Hunter's book (1).

Measurements of the streaming potential and pressure drop were conducted at five different channel heights ranging from 66 μm to 3 μm for three streaming solutions: 10^{-3} M KCl solution, 10^{-4} M KCl solution, and pure water. At each channel height the measurements were conducted over a number of pressures ranging from 2.4 kPa to over 50 kPa. The height of the channel was determined by relating volume flow rate measurements of a high concentration solution, thus no double layer effects, to h using Eq. [7] and was assumed to be accurate to within ± 0.2 μm.

4.2. Application of the Slope–Intercept Technique

Figures 5a, 5b, and 5c show the results of the streaming potential data collected for the pure water, 10^{-4} KCl, and 10^{-3} KCl streaming solutions respectively and the comparison between the different slope–intercept techniques and regression methods. In each case the average value of the parameter on the left-hand side of Eq. [13] and Eq. [30] over the range of pressures

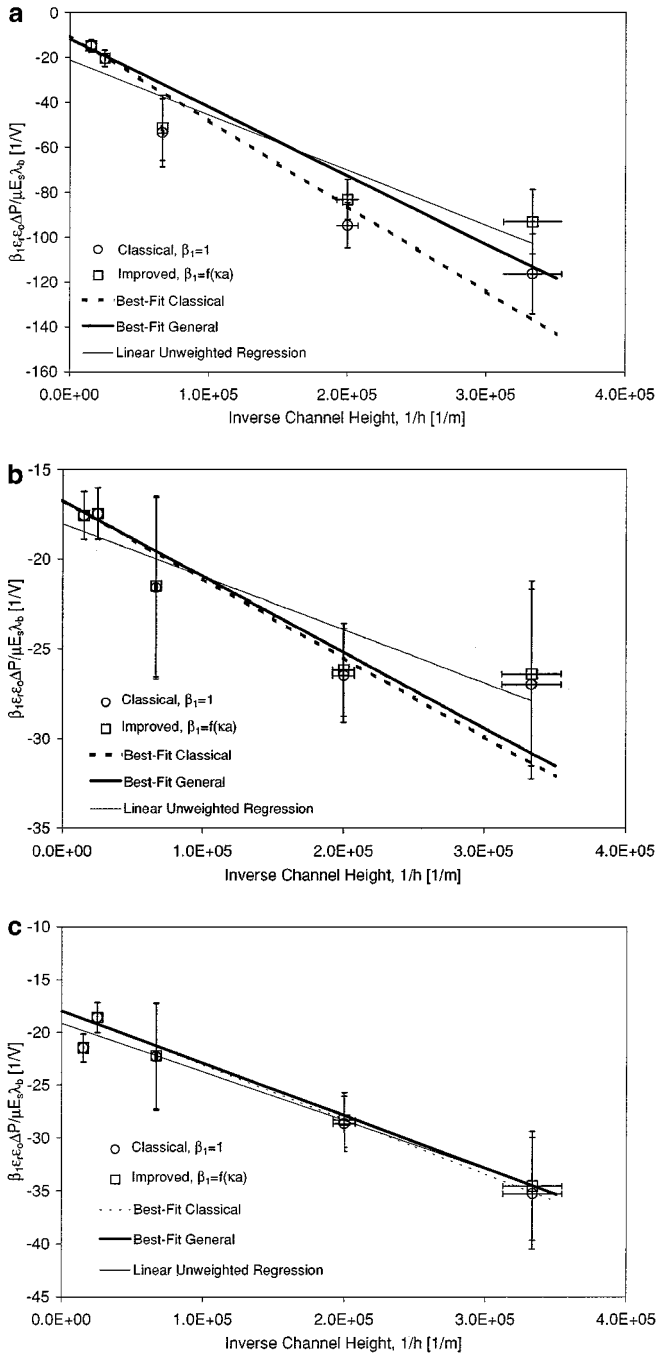

FIG. 5. (a) Comparison between the classical and the improved slope–intercept methods with the streaming potential data for glass surface in pure water. (b) Comparison between the classical and the improved slope–intercept methods with the streaming potential data for glass surface in a 10^{-4} M KCl solution. (c) Comparison between the classical and the improved slope–intercept methods with the streaming potential data for glass in a 10^{-3} KCl solution.

is shown and the error bars represent the standard deviation of all measurements. The viscosity was taken as 1.003×10^{-3} kg/ms; the dielectric constant, ε_r, and permittivity of free space, ε_o, were taken as 80 and 8.854×10^{-12} C/Vm. The bulk conductivity of the solutions was 0.1×10^{-3} S/m, 1.42×10^{-3} S/m and 14.2×10^{-2} S/m for pure water, 10^{-4} KCl M, and 10^{-3} M KCl solutions respectively.

In each of Figs. 5a, 5b, and 5c three regression lines are shown. The first (dashed line) is the best-fit line using the general least-squares algorithm presented in Section 3 applied to Eq. [13], the classical slope–intercept equation. The second (thick solid line) is the same algorithm applied to Eq. [30], or the improved slope–intercept equation. The linear unweighted line is the traditional least-squares algorithm, applied to the improved slope–intercept method. The results are summarized in Table 1.

Upon comparing Figs. 5a, 5b, and 5c, two points are immediately apparent:

(1) The lower the ionic concentration, the bigger the difference between the slope–intercept techniques and between the regression methods. So the error caused by the classical model and the unweighted regression method is large for pure water and dilute solutions.

(2) For a given solution, the smaller the channel height, the larger the difference between the classical and improved models, as shown by the distance between the data points marked by ○ (classical) and by □ (improved).

As mentioned in Section 2, the application of the β_1 correction factor will have two effects on the best-fit line: the y-intercept will be shifted down (i.e., more negative) and the slope will be less severe. By examining Figs. 5a, 5b, and 5c or Table 1 this is indeed apparent in each case; however, it is only significant for pure water. For that case β_1 ranges from 0.98 for the largest channel to 0.8 for the smallest, resulting in the significant differences between the classical and modified data points observed at the smaller channels sizes in Fig. 5a. As a result the classical method overestimates the ζ-potential by 12.5% and the surface conductance by 35%. In the higher concentration cases, where double layer effects are less significant and β_1 approaches unity, the differences are less significant and in fact nearly disappear for the case of the 10^{-3} M solution.

As alluded to earlier since β_1 is less than unity the improved method will always reduce the magnitude of the dependent parameter and shift the data points up on the chart. While large

TABLE 1

Results of the Least-Squares Analysis and the Two Slope–Intercept Methods Applied to the Streaming Potential Data of the Glass Surface–Solution Systems

		Intercept	Slope	ζ (mV)	λ_s (nS)
Pure water (Fig. 5a)	Improved	−11.67	-3.05×10^{-4}	−86	1.31
	Classical	−10.31	-3.80×10^{-4}	−97	1.84
	Unweighted	−21.24	-2.44×10^{-4}	−47	0.58
10^{-4} KCl (Fig. 5b)	Improved	−16.88	-3.91×10^{-5}	−59	1.64
	Classical	−16.87	-4.10×10^{-5}	−59	1.73
	Unweighted	−18.02	-2.96×10^{-5}	−55	1.16
10^{-3} KCl (Fig. 5c)	Improved	−17.96	-5.02×10^{-5}	−56	19.8
	Classical	−17.94	-5.22×10^{-5}	−56	20.7
	Unweighted	−19.14	-4.59×10^{-5}	−52	17.0

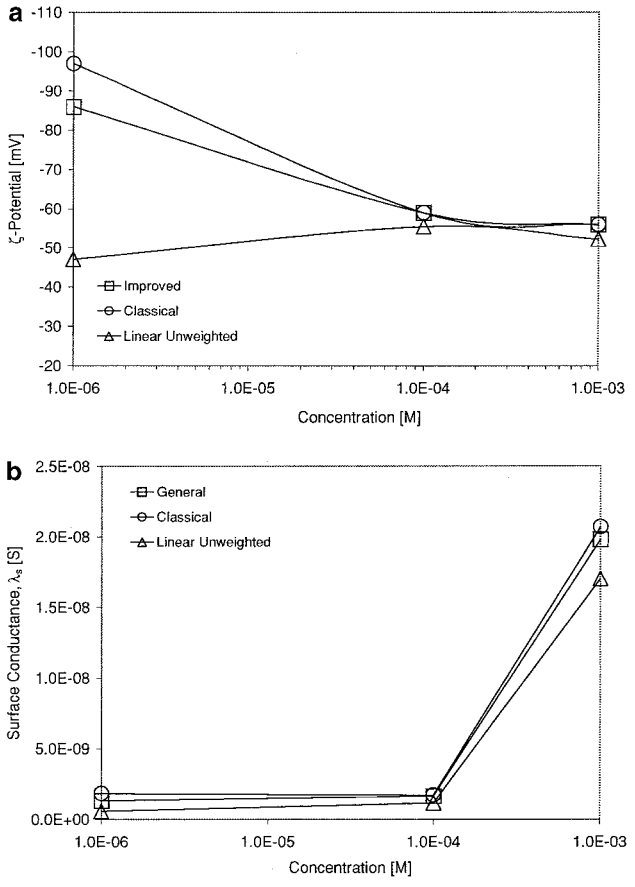

FIG. 6. (a) Variation of ζ-potential with ionic concentration for different slope–intercept techniques. (b) Variation of surface conductance with ionic concentration for different slope–intercept techniques.

differences are noticeable in Fig. 5a the other two figures show relatively minor differences, even at the smaller channel heights. As a result it can be concluded that at these concentrations the EDL has little effect on the flow or the velocity profile.

The other consequence of the improved slope–intercept method was the slope correction, which results from the electroosmotic back-pressure on the flow. The value of this correction is -1.15×10^{-6}, -6.85×10^{-7}, and -6.38×10^{-8} for the pure water, 10^{-4} M, and 10^{-3} M KCl solutions respectively, which are all less than 1% of the observed slope. Thus, for this example the electroosmotic back-pressure can be effectively ignored; however, in cases where surface conductance is very low or ζ-potentials very high this correction must be considered.

Figures 6a and 6b show the variation in the ζ-potential and surface conductance with ionic concentration, for each of the three methods outlined above. While both Eq. [13] and Eq. [30] computed with the general regression technique show the expected decrease in ζ-potential with increasing ionic concentration, it is apparent that the traditional regression technique has yielded a physically inconsistent result with the lowest ζ-potential occurring for pure water. This is the result of the traditional technique placing too much weight on the measurements made at the smaller channels where the uncertainty is the greatest. Unlike the ζ-potential, as ionic concentration increases the surface conductance should also increase. From Fig. 6b it is apparent that all three methods predict a significant increase in the surface conductance as the ionic concentration increases from 10^{-4} M to 10^{-3} M. Comparing the results of the 10^{-6} M and the 10^{-4} M solutions from Table 1, however, it is interesting to note that while the improved approach shows an increasing trend the classical solution suggests that λ_s will remain about the same; in fact it actually decreases a small amount. This is a result of the classical technique overestimating the surface conductance at the lowest concentration.

By examining the error bars in each of Figs. 5a, 5b, and 5c it becomes apparent that the standard deviation, and therefore uncertainty, of the measurements made at each channel height are not the same. The *x* error bars show that as the channel height decreases the significance of the ± 0.2 μm uncertainty becomes quite consequential, in extreme cases nearing the magnitude of the *y* uncertainty. By examining the *y* error bars it is apparent that all the data points do not show equal variance and thus should not be given equal weight. As a result the assumptions required for the traditional regression method (see Section 3) to be applicable are not met in this case and in fact that algorithm yields results dramatically different than those obtained from the more general method as mentioned earlier.

4.3. Uncertainty Analysis

Critical to any statistical curve-fitting analysis is the certainty with which the parameters can be said to be accurate. This is done with a *t*-test as described in Section 3.2. Such an analysis has been performed here for all three regressed lines to the 90% confidence level and the results are shown in Table 2.

For the higher concentration solutions, 10^{-3} M and 10^{-4} M, this method has yielded the true value of the ζ-potential for the solid surfaces to within ± 5 mV with 90% confidence. Similarly for the two lowest concentration solutions, 10^{-6} M and 10^{-4} M, it can be said with 90% confidence that the true value surface conductance is within $\pm 1 \times 10^{-9}$ S of that shown in Table 2.

The most significant result of the error analysis is the uncertainty of the ζ-potential result for the case of pure water. There

TABLE 2
90% Confidence Levels on ζ and λ_s Results of the Glass Surface–Solution Systems

		ζ (mv)		λ_s (nS)	
		Low	High	Low	High
Pure water (Fig. 5a)	Improved	−54	−201	0.9	1.7
	Classical	−63	−209	1.4	2.3
	Unweighted	−23	+2090	0.3	0.9
10^{-4} KCl (Fig. 5b)	Improved	−55	−64	1.1	2.2
	Classical	−55	−64	1.2	2.3
	Unweighted	−47	−67	0.5	1.8
10^{-3} KCl (Fig. 5c)	Improved	−61	−51	10.4	29.3
	Classical	−61	−51	11.1	30.3
	Unweighted	−58	−47	13	21

are two major reasons for this. First the standard deviation of the intercept, as calculated by Eq. [41], was much larger in this case than in the other two examples, likely due to the relatively large uncertainty in the measurements made at smaller channels. Also contributing to the large confidence range, however, is the stability of the solution at high ζ-potentials. Since the ζ-potential is the inverse of the y-intercept it is obvious that such cases will have intercepts very near $y = 0$. Near $y = 0$ a small change in the intercept will have a large effect on the ζ-potential. For example, a ζ-potential of -200 mV coincides with a y-intercept of -5; if the confidence level on intercept is ± 2 units the range of ζ-potentials would be from -142 mV to -333 mV, a span of 190 mV. If the same level of confidence is placed on an intercept of -20, the range of ζ-potentials is much smaller at -45 mV to -55 mV, a range of only 10 mV. Thus a high ζ-potential is bound to be much more unstable than a low ζ-potential. This is well demonstrated for the case of interest by the asymmetry in the confidence range since the lower 90% confidence value is 32 mV below the mean and the upper is 115 mV above it.

In the above section the slope–intercept method has been applied to streaming potential measurements made on glass surfaces for three different streaming solutions. In all cases the classical method overestimated the value of the ζ-potential and surface conductance, with the most significant differences observed for the case of pure water. When the ionic concentration was increased the improved and classical methods converged to the same solution even when relatively small channels were used to make the measurements. It was also shown that at higher ζ-potentials the stability of the solution can be a problem and uncertainties are likely to be larger than those for low ζ-potentials.

5. SUMMARY

Electrokinetic characterization of solid surfaces is important to a number of fields in engineering and the physical sciences. The slope–intercept method is a technique by which the ζ-potential and surface conductance, λ_s, can be determined from streaming potential measurements conducted at different channel heights. In the classical form of the technique, the parameter $\varepsilon_r\varepsilon_o\Delta P/\mu E_s\lambda_b$ is plotted as a function of the inverse channel height, $1/h$, and ζ and λ_s are then determined from the slope and intercept of a best-fit line through these points. The above form of this technique is derived on the basis of assumptions that are in general not true for small parallel plate channels in solutions of low ionic concentration.

In this paper an improved slope–intercept technique has been developed which accounts for cases where the EDL or the electrokinetic effect on the flow is significant. Additionally, a general least-squares regression analysis is discussed as well as the proper technique for estimating the confidence in the final solution. To account for the more general conditions two correction factors were introduced to the classical technique. The first was a correction applied to the $\varepsilon_r\varepsilon_o\Delta P/\mu E_s\lambda_b$ parameter, which accounted for the effect of small channel height or relatively thick EDL. As expected this correction became was very significant in small channels in low concentration solutions. Since this correction was always less than unity it was concluded that the classical technique would overestimate the ζ-potential and surface conductance. The second correction accounted for the electroosmotic back-pressure on the fluid in the channel. As was shown the magnitude of this correction is approximately linear with channel height and it must be subtracted from the slope prior to the computation of the surface conductance, leading to a further overestimation of the surface conductance by the classical technique. Such a correction would be very significant in cases of very low surface conductance.

In this paper, streaming potential data obtained for glass surfaces in a variety of solutions ranging in ionic concentration from 10^{-6} M to 10^{-3} M are presented. When the two methods were applied to experimental streaming potential data, it was confirmed that the classical technique indeed overestimates both the ζ-potential and surface conductance of the solid surface. In solutions of low ionic concentration, nearing that of pure water, this overestimation was shown to be quite significant. As the solution ionic concentration increased and the thickness of the double layer diminished, the two methods were shown to produce nearly identical results.

The traditional regression technique, which assigns equal weight to all data points and ignores uncertainty in the independent measurement, was shown to be inadequate when applied to experimental data and in some cases produced physically inconsistent results. As such it is recommended that the more general technique described here should be used. Examining the 90% confidence range in the fitted parameters suggested that solution instability may be a problem at higher ζ-potentials since small changes in the y-intercept can result in significant errors in ζ.

APPENDIX

As mentioned in Section 3 the line of best-fit required for the slope–intercept method is found using a general least-squares analysis which determines the values of the fitted parameters that minimize the sum of squares of the error between the measured and predicted values. For the general case where statistical weighting is used and errors in the independent variables are considered it was shown that the best-fit values of the slope, α_1, and intercept, α_2, are those which satisfy Eq. [A1.1]:

$$\frac{1}{2}\delta S = \sum_{i=1}^{n}\left(w_{y_i}R_{y_i}\delta R_{y_i} + w_{x_i}R_{x_i}\delta R_{x_i}\right) = 0. \quad \text{[A1.1]}$$

The solution to Eq. [A1.1] begins by defining a conditional function, F_i, for each of the measured data points,

$$F_i = Y_i - f(X_i;\alpha_1,\alpha_2) = Y_i - \alpha_1 X_i - \alpha_2 \neq 0, \quad i = 1, 2, \ldots n, \quad \text{[A1.2]}$$

where the uppercase Y_i and X_i are the measured values corresponding to the ith data point and α_1 and α_2 are the initially guessed values of the slope and y-intercept. The above expression is expanded in a Taylor series about the point where $F_i = 0$,

yielding

$$F_i = \frac{\partial F_i}{\partial Y_i} R_{y_i} + \frac{\partial F_i}{\partial X_i} R_{x_i} + \frac{\partial F_i}{\partial \alpha_1} A_1 + \frac{\partial F_i}{\partial \alpha_2} A_2 = R_{y_i} - \alpha_1 R_{x_i} - X_i A_1 - A_2, \quad i = 1, 2, \ldots n, \quad [A1.3]$$

where A_1 and A_2 are given by

$$A_k = \alpha_k|_{\text{old}} - \alpha_k|_{\text{new}}, \quad k = 1, 2. \quad [A1.4]$$

Varying the residuals of Eqs. [A1.4] so that the conditional functions are made equal to zero yields Eqs. [A1.5],

$$0 = \delta R_{y_i} - \alpha_1 \delta R_{x_i} - X_i \delta A_1 - \delta A_2, \quad i = 1, 2, \ldots n. \quad [A1.5]$$

Using the method of Lagrange multipliers, each of Eqs. [A1.5] is multiplied by a different multiplier, λ_i, and then subtracted from Eq. [A1.1], yielding

$$\sum_{i=1}^{n} \left(w_{y_i} R_{y_i} - \lambda_i\right) \delta R_{y_i} + \sum_{i=1}^{n} \left(w_{x_i} R_{x_i} + \lambda_i \alpha_1\right) \delta R_{x_i} + \sum_{i=1}^{n} \lambda_i X_i \delta A_1 + \sum_{i=1}^{n} \lambda_i \delta A_2 = 0. \quad [A1.6]$$

Since the variations are arbitrary, Eq. [A1.6] is satisfied only when

$$R_{y_i} = \frac{\lambda_i}{w_{y_i}}, \qquad i = 1, 2, \ldots n \quad [A1.7a]$$

$$R_{x_i} = -\frac{\lambda_i \alpha_1}{w_{x_i}}, \quad i = 1, 2, \ldots n \quad [A1.7b]$$

$$\sum_{i=1}^{n} \lambda_i X_i = 0, \quad [A1.7c]$$

$$\sum_{i=1}^{n} \lambda_i = 0. \quad [A1.7d]$$

Conditions [A1.7a] and [A1.7b] can then be substituted into Eq. [A1.3] to obtain

$$F_i = \frac{\lambda_i}{w_{y_i}} + \frac{\lambda_i \alpha_1^2}{w_{x_i}} - X_i A_1 - A_2, \quad i = 1, 2, \ldots n. \quad [A1.8]$$

Equation [A1.8] can be simplified by defining the following function,

$$L_i = \frac{1}{w_{y_i}} \left(\frac{\partial F_i}{\partial y}\right)^2 + \frac{1}{w_{x_i}} \left(\frac{\partial F_i}{\partial x}\right)^2 = \sigma_{y_i}^2 + \left(\alpha_1 \sigma_{x_i}\right)^2, \quad i = 1, 2, \ldots n. \quad [A1.9]$$

Substituting Eqs. [A1.9] into Eqs. [A1.8] and solving for λ_i yields

$$\lambda_i = \frac{1}{L_i}(F_i + X_i A_1 + A_2), \quad i = 1, 2, \ldots n. \quad [A1.10]$$

Substituting Eqs. [A1.10] into conditions [A1.7c] and [A1.7d] yields a set of two equations and two unknowns, which is most often expressed as

$$CA = V \quad [A1.11a]$$

$$C = \begin{bmatrix} \sum_{i=1}^{n} \frac{X_i^2}{L_i} & \sum_{i=1}^{n} \frac{X_i}{L_i} \\ \sum_{i=1}^{n} \frac{X_i}{L_i} & \sum_{i=1}^{n} \frac{1}{L_i} \end{bmatrix} \quad [A1.11b]$$

$$V = -\begin{bmatrix} \sum_{i=1}^{n} \frac{X_i F_i}{L_i} \\ \sum_{i=1}^{n} \frac{F_i}{L_i} \end{bmatrix}. \quad [A1.11c]$$

Equation [A1.11] can then be solved directly for the values of A_1 and A_2, which are then related to the least-squares best-fit parameters through Eq. [A1.4]. Since the value of α_1 in Eqs. [A1.2] is only an approximation it is apparent that the Taylor expansion is not exact and the above procedure must be repeated with the updated value of α_1 until such time as the solution is converged upon to an acceptable tolerance. When $R_{x_i} = 0$, such as is the case in the traditional least-squares analysis, Eqs. [A1.2] are exact and Eq. [A1.11] will yield the best-fit values of α_1 and α_2 directly.

ACKNOWLEDGMENTS

The authors thank the Natural Sciences and Engineering Research Fund for financial support through scholarships to D.E. and through a research grant to D.L.

REFERENCES

1. Hunter, R. J., "Zeta Potential in Colloid Science, Principals and Applications." Academic Press, New York, 1981.
2. Sanders, R. S., Chow, R. S., and Masliyah, J. H., *J. Colloid Interface Sci.* **174,** 230 (1995).
3. Jones, G., and Wood, L., *J. Chem. Phys.* **13,** 106 (1945).
4. Van Wagenen, R. A., and Andrade J. D., *J. Colloid Interface Sci.* **76,** 305 (1980).
5. Voight, A., Wolf, H., Lauckner, S., Neumann, G., Becker, R., and Richter, L., *Biomaterials* **4,** 299 (1983).
6. Jacobasch, H.-J., and Schurz, J., *Prog. Colloid Polym. Sci.* **77,** 40 (1988).
7. Gu, P., and Li, D., *J. Colloid Interface Sci.* **226,** 328 (2000).
8. Werner, C., Körber, H., Zimmermann, R., Dukhin, S., and Jacobasch, H.-J., *J. Colloid Interface Sci.* **208,** 329 (1998).
9. Briggs, D., *J. Phys. Chem.* **32,** 641 (1928).
10. Rutgers, A., *Trans. Faraday Soc.* **36,** 69 (1940).
11. Wolberg, J., "Prediction Analysis." Van Nostrand, Princeton, NJ, 1967.